Nanoscale

PAPER

View Article Online
View Journal | View Issue

Cite this: *Nanoscale*, 2020, **12**, 3482

Direct identification of the herpes simplex virus *UL27* gene through single particle manipulation and optical detection using a micromagnetic array†

Peng Li,[a] Dhruv Gandhi,[a] Marina Mutas,[a] Yin-Fen Ran,[a] Michael Carr,[b,c] Stefano Rampini,[a] William Hall[b] and Gil U. Lee *[a]

Received 18th December 2019,
Accepted 16th January 2020

DOI: 10.1039/c9nr10362g

rsc.li/nanoscale

Magnetophoretic lab on a chip technologies are rapidly evolving into integrated systems for the identification of biomarkers and cells with ultra-high sensitivity. We demonstrate the highly efficient detection of the Human herpes simplex virus type 1 (HSV) *UL27* gene through the programmed assembly of superparamagnetic (SPM) nanoparticles based on oligonucleotide hybridization. The state of assembly of the SPM nanoparticles was determined by optical signature of the synchronized motion on the beads on a micromagnetic array (MMA). This technique has been used to identify <200 copies of the HSV *UL27* gene without amplification in less than 20 minutes. The MAA can also be used to separate gene-SPM bead aggregates from millions of unreacted SPM beads based on nonlinear magnetophoresis (NLM). The MMA-optical detection system promises to enable highly sensitive, nucleic acid analysis to be performed without amplification and with the consumption of minimal amounts of reagent.

Introduction

SPM nanoparticles are widely used *in vitro* diagnostics as they facilitate rapid transferred of specific protein, viruses or cells into a device for analysis. Research in lab on a chip (LOC) technologies initially focused on implementing high-gradient magnetic field separation on-chip due to the well-established role that this technology.[1–4] For example, glass and antibody coated SPM nanoparticles are widely used to rapidly isolate nucleic acids from cell lysates and rare cell-types from serum, respectively.[5–8] The favourable scaling of the magnetophoretic separation velocity (v) makes it possible to complete on-chip separations a matter of minutes, *i.e.*,

$$v \propto \frac{F}{6\pi\eta R} = \frac{R^2\chi\nabla B^2}{9\mu_o\eta}, \quad (1)$$

where F is magnetic force, η is viscosity, R is the radius of the SPM nanoparticle (which can vary between 50–5000 nm), χ is the magnetic susceptibility of the SPM composite, μ_o is the magnetic permeability of free space and ∇B is the magnetic flux density. Manipulation of SPM nanoparticles in LOC instruments has also been facilitated by using electromagnets to time reaction and separation steps. Magnetophoretic LOC point of care tests (POCTs) have enabled rapid and sensitive detection of biomarkers and cells, consuming minimal volumes of reagents.[9]

Significant advances in the function and performance of magnetophoretic LOC devices has resulted from their integration with highly sensitive detectors. Spintronic materials, developed for hard disc read-write heads and magnetoresistive random-access memory applications, have been used to detect SPM nanoparticles at the surface of LOC devices with a high degree of specificity and sensitivity. LOC devices based on arrays of highly sensitive giant magnetoresistance, tunnel magnetoresistance and planar hall resistance detectors have advanced to the stage where it is now possible to detect single 60 nm SPM particles bound to 64 sensor arrays.[3,10–12] Integrated systems with these sensors have been fabricated and used to detect single cells and low-affinity protein–protein interactions.[13–15] These highly innovative devices are currently limited, however, by the total number of particles that they can work with and thus the types of samples that they can be used to analyze.

Programmed SPM nanoparticle actuation has been achieved with micron resolution using micromagnet

[a]*School of Chemistry and Chemical Biology, University College Dublin, Belfield, Dublin 4, Ireland. E-mail: gil.lee@ucd.ie*
[b]*UCD National Virus Reference Laboratory, University College Dublin, Belfield, Dublin 4, Ireland*
[c]*Global Station for Zoonosis Control, Global Institution for Collaborative Research and Education (GI-CoRE), Hokkaido University, Sapporo 001-0020, Japan*
†Electronic supplementary information (ESI) available. See DOI: 10.1039/c9nr10362g

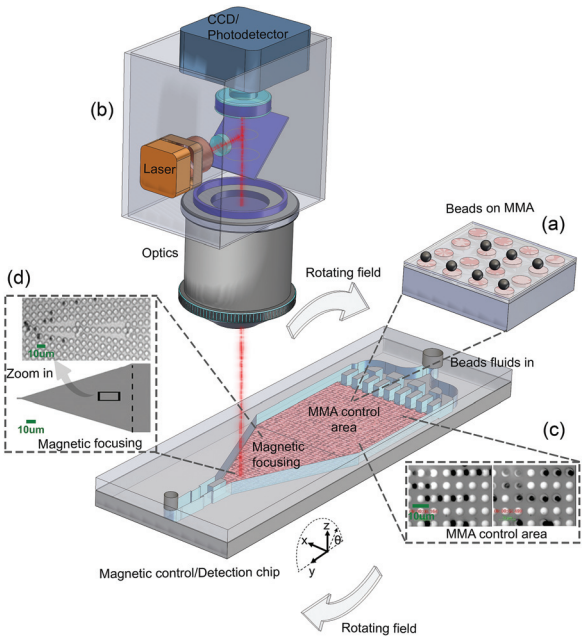

Fig. 1 Magnetophoretic separation of superparamagnetic particles on a micromagnet array (MMA) with a magneto-optical detection system. (a) Schematic of the SPM particles moving over 5 μm diameter circular micro-magnet mirrors. (b) Schematic of the magneto-optical detection system, which is composed of a laser, focusing optics, photodetector, and MMA. (c) Optical microscope image of a set of 2.8 μm SPM particles (black circles) moving across an array of the circular micromagnet mirrors (white circles) with an external magnetic field orientation of θ = 0° (left) and θ = 180° (right). (d) Schematic and optical images of a MMA element that can be used to focus SPM particles.

arrays.[13,16–18] Fig. 1 presents a schematic of an instruments that uses a rotation external magnetic field to actuate more than 10^6 SPM particles on a MMA of centimeter size. The SPM particles are trapped in the strong localized magnetic field surrounding the micro-magnets, which minimizes magnetic interactions for SPM particles that have a $\chi < 1$. At low frequencies the particles move across the micromagnet array at a rate that is defined by the rotating external magnetic field. For example, the counter-clockwise rotation of the external magnetic field in the *yz*-plane of the array results in the movement of the SPM particles in the *y*-direction. The SPM particle's motion is determined by its hydrodynamic size and the magnetic force. This results in a critical frequency, ω_c, at which an SPM particle can no longer closely follow the external magnetic field due to the hydrodynamic drag force.[19] The magnitude of ω_c has been found to increase with the magnetic moment of the SPM particle but is a nonlinear function of its hydrodynamic radius:

$$\omega_c = \frac{X\mu_o\sigma_o H}{18\eta}\,(2\pi\beta)^2 e^{-2\pi\beta}, \qquad (2)$$

where σ_o is the effective magnetic moment of the micromagnetic, η is the viscosity of the sample, and β is the ratio of the particle's radius and the center-to-center distance between the magnets. The strong dependence of the critical frequency on hydrodynamic drag can be used to separate SPM nanoparticles of different sizes, *i.e.*, SPM particles with a $\omega < \omega_c$ will move on the magnetic arrays, while particles that have a $\omega > \omega_c$ will slow down and become immobilized at the immobilization frequency, ω_i. Nonlinear magnetophoresis on a MMA of centimeter size has been used to separate 10^6 SPM nanoparticles based on their size or magnetization. This technique has been used to isolate bacteria and exosome-SPM particle complexes based on the decrease in the magnetization of the complexes.[20] MMAs have also been used to collect cells bound to SPM nanoparticles and focus them into specific channels like those shown in Fig. 1d for analysis.[21] Integration of these devices with detectors promises to allow POCT and *in vitro* assays to be rapidly performed directly from complex biological samples.

In this article we demonstrate the principle of direct nucleic acid identification, *i.e.*, without amplification, of an open reading frame derived from HSV-1 based on SPM nanoparticle reaction, separation and detection. HSV is a large (>150 kb), double-stranded DNA virus that is transmitted to humans by direct skin to skin contact; in the case of HSV-1 by contact with the orofacial region, and for HSV-2 through sexual routes. Between 60%–95% of adults worldwide are infected by HSV.[22] Initial symptoms include sores or blisters around the infected region, causing discomfort and in some cases, pain, for the individual. Although rare, HSV-2 infection of the central nervous system can occur, resulting in herpes simplex encephalitis (HSE), which is fatal in 70% of untreated cases.[23] There has been a growing awareness that HSV-1 infections may be linked to a number of neurodegenerative diseases.[24] The clinical outcome of HSV infection can be favorable if antiviral therapy is initiated in the early stages of infection, accentuating the need for rapid diagnostic assays. Viral loads in clinical samples (cerebrospinal fluid, plasma, genital and oral swabs) and are typically in the range 10^2–10^6 DNA copies per ml.[25] The gold standard HSV diagnostic test involves the monitoring of cytopathic effects of the virus following inoculation on susceptible cell cultures. While highly sensitive and specific, results can take up to one week to complete.[26] To circumvent time issues, polymerase chain reaction (PCR), has been proposed as an alternative diagnostic assay, which maintains high sensitivity and specificity, but requires trained personnel and remains time consuming (4 h).[27] Other diagnostic procedures such as enzyme immunoassay and fluorescent antibody tests typically take several hours to conduct and suffer from poor sensitivity.[28,29]

The identification of HSV-1 was based on a highly efficient reaction of the *UL27* gene with SPM nanoparticles and the use of an MMA for separation and optical detection of the aggregation state of the particles. In the magnetic bead assembly (MBA) assay the HSV *UL27* gene was labelled with biotin and digoxigenin (dig) oligonucleotide probes and rapidly separated with streptavidin and anti-dig antibody labeled SPM nanoparticles. The use of a high concentration of SPM nanoparticles and magnetic manipulation allowed each of these reactions to be efficiently completed in high levels of back-

ground DNA in as little as 2 minutes.[30] Detection of SPM bead assemblies was performed using a novel optical detection scheme that is capable of identifying individual SPM particles and their aggregation state. This technique allowed the *UL27* gene to be detected at a copy number of <200 without amplification and promises to be highly useful for POCT where a rapid response is required. It also provides the means for directly identifying modified DNA that are not easily detected using PCR, *e.g.*, 5-methylcytosine modification of DNA could be detected for epigenetic profiling if methylated binding proteins are used.

Experimental

Micromagnetic optical detection system

The MMA was fabricated from 5 μm diameter circular micromagnet mirrors arranged in a rectilinear pattern of 8 μm period using a conventional lift-off processing.[20] To achieve high reflectivity and anisotropic magnetic moment the MMA were fabricated from a stack of reflective and magnetic layers, *i.e.*, 10 nm chromium, 100 nm cobalt, and 10 nm chromium, deposited on a silicon substrate. Fig. 1(a) and (b) present optical micrographs of 2.8 μm SPM particles moving across a MMA as an external magnetic field that was rotated in the *xz*-plane. The transport of the SPM particles on the MMA was characterized with a reflected light microscope equipped with a high-speed camera (Axiocam, Zeiss), as shown in Fig. 1d. The external magnetic field was generated with *y* and *z*-oriented electromagnets that were driven with two sinusoidal signals that were 90° out-of-phase. The synchronized signals were amplified to the desired current using two programmable amplifiers (Kepco, Flushing, NY) to produce a maximum field of approximately 60 gauss. Magneto-optical detection of the SPM particle transport was performed on-chip with a 635 nm, 15 mW AlGaInP laser diode (Hitachi HL6322G). The laser was focused through a 63x microscope objective (Zeiss Plan-Neofluar, NA = 0.75) using a collimating lens (Linos A240A, Munich, Germany) resulting in a 256 μm diameter spot size. The light collected from the MMA was detected with a switchable gain photodetector with built-in amplifier (2.4 MHz BW, 75 mm^2, 70 dB switchable gain, PDA100a Thorlabs).

Optimization of the magnetic bead assembly (MBA) assays

The principle of the MMA detection was initially demonstrated using a three-step MBA assay to detect the model protein biotinylated bovine serum albumin (BBSA) based on the aggregation of streptavidin SPM particles.[30] The assay was performed by adding streptavidin SPM particles to BBSA solutions of defined concentration to achieve a final particle concentration of 10^7 ml^{-1}. The solution was incubated at room temperature for 5 min and then subjected to magnetic field activated aggregation, *i.e.*, the sample was placed in a 2.5 kGauss magnetic field for 1 minute at which time most of the particles came out of solution. These samples were immediately analyzed with either the magneto-optical detector or a flow cytometry (Accuri C6, Becton Dickson). For the magneto-optical detection analysis a 10 μl volume of sample was injected onto the MMA and the measurement was initiated after allowing the particles to settle for 1 minute. Flow cytometry analysis was carried-out by collecting at least 10 000 events with a threshold of 80 000 relative intensity units (RIU) on the forward scatter light-height (FSC-H) channel. Monomers and aggregate populations were identified by using the FSC-H *versus* area (FSC-A) channel. Total assay times were 15 minutes.

The HSV *UL27* gene MBA assay was developed in three phases to optimize the hybridization and SPM particle reactions. In the first phase a 25-base pair (bp) DNA oligonucleotide was detected that was 5′ labeled with biotin and dig using streptavidin and anti-dig functionalized SPM particles. The double-stranded (ds) biotin-25mer-dig was formed by hybridization of the complementary biotin-HSV-gab(+) and dig-HSV-gBE(−) oligonucleotides (Table S1, ESI†) at a temperature 10 °C greater than their T_m in 1× annealing buffer (10× annealing is 10 mM Tris-HCL, pH 7.5, 100 mM NaCl, 1 mM EDTA). Fig. S2 (ESI†) presents the results of this MBA assay, which can detect the 25mer at 10^{-13} M of dsDNA. The MBA assay was found to have the highest sensitivity and lowest background for 2 min reaction times (Fig. S3†) for equal concentrations of streptavidin and anti-dig SPM particles at a particle concentration 7×10^6 ml^{-1} (Fig. S5†). This level of sensitivity could be achieved even in a high levels of background DNA, *i.e.*, 20 mg ml^{-1} concentrations of bovine serum albumin or salmon sperm DNA (Fig. S5†). In the second phase of assay optimization two 25-mer oligonucleotide probes, *i.e.*, the 3′-labled biotin-HSV-1P1 and 5′-labeled dig-HSV-1P1 (Table S1†) were hybridized with a 75-mer synthetic fragment of the (−) strand of the HSV-1 *UL27* gene at 60 °C. The DNA product was composed of two labeled ds 25-mers separated by a 25 bp single strand. Fig. S5† presents the MBA detection of the HSV-1 *UL27* (−) strand using the optimized reaction conditions. In the final assay, the HSV *UL27* gene was directly detected in its double stranded form, *i.e.*, the target dsDNA *UL27* gene was formed by hybridizing equimolar quantities of HSV *UL27* gB- and HSV-1 *UL27* gB-oligonucleotides at 10 °C above their T_m's. The dsDNA *UL27* gene fragment was hybridized with 10^{-8} M concentrations of the biotin-HSV-1P1 and dig-HSV-1P1 oligonucleotide probes at 80 °C in 1× annealing buffer. This construct was detected by reacting it with streptavidin and anti-dig SPM particles using reaction conditions developed first phase of reaction optimization.

Preparation of SPM particles

Three types of 2.8 μm diameter SPM particles were used in this study, *i.e.*, carboxyl, streptavidin, and antibody functionalized polymer particles in which nanometer iron oxide nanoparticles are distributed. The carboxyl and streptavidin particles were used as received from the manufacture (Dynal, Invitrogen). Anti-digoxigenin functionalized particles were synthesized by reacting the biotinylated antibody (Abcam, Cambridge, UK) with the streptavidin functionalized particles (Table S2† presents information about the antibodies). This was achieved by reacting the anti-dig antibody at 0.1 mg mL^{-1}

with the streptavidin particles (3 mg) in 800 μL PBS buffer for 1 h at room temperature. After incubation, the antibody coated particles were washed with PBST buffer, incubated with an excess of 10 μg ml^{-1} of biotin and stored with PBST with 0.1 (wt/wt%) BSA at 4 °C.

Results and discussion

Optical detection of SPM particles on MMAs

Fig. 2a presents the intensity of the reflected light signal resulting from the motion of the carboxyl functional SPM particles moving across a MMA (red) and silicon surface (blue) in a rotating magnetic field as a function of frequency, *i.e.*, ω = 0, 1, 5–15 and 30 Hz. The strong periodic signal on the MMA was synchronized with the external magnetic field and was observed on a background signal of ~425 mV. This periodic signal was not sinusoidal but moved through four levels as the external magnetic field was varied from 0, 90, 180, and 270° in the *yz*-plane (inset Fig. 2b). These observations led us to concluded that the strong optical signal resulted from the synchronized motion of the particles across the MMA, *i.e.*, the particles were either located above the silicon surface or over a micromagnet, as shown in Fig. 1c and Movie 1 (ESI†).

The magnitude of the peak-to-peak photodetector signal, V_{pp}, was found to be sensitive to the frequency of rotation of the external magnetic field, as shown in Fig. 2b. At frequencies less than 15 Hz, the magnitude of V_{pp} did not vary with ω but was observed to decrease at frequencies above 15 Hz, ultimately reaching a value close to zero above 30 Hz. This behavior is closely related to the transport of the SPM particles across the MMA, which was characterized by the critical frequency, ω_c = 20 Hz, and the immobilization frequency, ω_i, = 30 Hz (as described below). The decrease in the magnitude of V_{pp} at frequencies greater than 15 Hz resulted from the fact that a significant portion of the SPM particles lost their ability to follow the time varying magnetic field. The portion of asynchronized particles increased with frequency until they were largely immobilized at ω_i. A time varying signal can also be detected for particles moving on the bare silicon substrates (*i.e.*, without micromagnets) in the rotating magnetic field, but it was significantly weaker than that measured on the MMA (Fig. 2a). This signal resulted from the tumbling of multimeric linear SPM particle assemblies on the substrate, which formed due to the strong long-range magnetic forces that occur between SPM particles in an external magnetic field.[31]

This magneto-optical detector signal was also strongly dependent on the concentration of SPM particles added to the MMA. Fig. 2b also presents the V_{pp} for concentrations of SPM particles varying from 10^6 to 2 × 10^7 ml^{-1} as ω was increases from 0 to 40 Hz (*i.e.*, the number of beads in the detector area varied between 10 and 100). Two features of the frequency response can be observed in these measurements. First, the V_{pp} signal increased as the density of particles on the MMA increased at frequencies below the immobilization frequency. Second, at frequencies above ω_c the V_{pp} rapidly decreased, ulti-

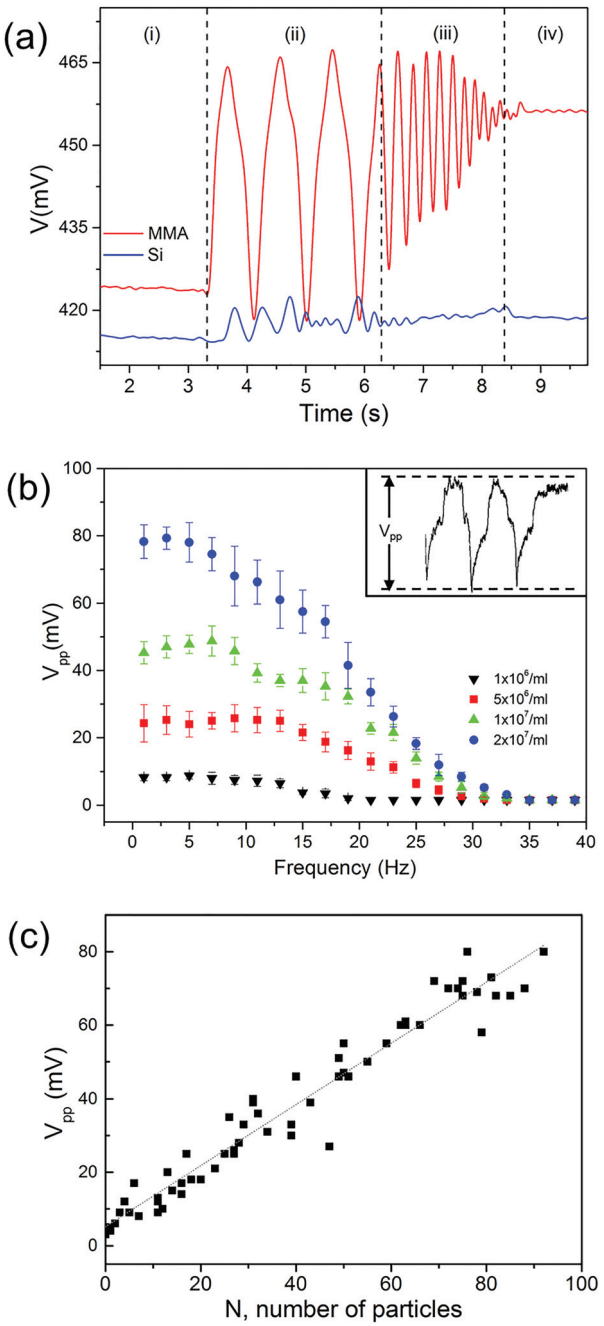

Fig. 2 Detection of superparamagnetic particle on a MMA. (a) Photodetector signal resulting from the transport of SPM particles on a MMA (added at a concentration of 10^6 ml^{-1}) as function of the frequency of rotation of the external magnetic field ω. Red curve is for motion of the particles on MMA and blue curve is for the particles on a bare silicon surface (i) without rotating magnetic field, (ii) ω = 1 Hz, (iii) ω = 5–15 Hz, and (vi) ω = 30 Hz. (b) Peak-to-peak voltage (V_{pp}) of photodetector signal as function of ω as the concentrations of particles added to the MMA are increased from 10^6 to 2 × 10^7 ml^{-1} (10 μl of beads were placed on a 1 × 1 cm MMA). At least 5 measurements were made for each data point plotted. Inset shows definition of V_{pp} as a characteristic parameter in photodetector signal. (c) V_{pp} measured as a function of the number of particles (N) in the optical detection area. The response is linear V_{pp} = 5.15 + 0.83N where R^2 = 0.90903.

mately reaching a value that was independent of the density of particles at ω_i. This is consistent with our observation that the response of the detector was closely related to the transport of the SPM particles on the MMA. Microscopic examination of the SPM particles on the MMA at ω_i revealed that they were immobilized between the micromagnets.

Fig. 2c presents the magneto-optical detector signal for intensity of light reflected from SPM particles on a MMA at 1 Hz as the number of particles in the field of detection, N, increased from 0 to 100. At this low frequency, all the SPM particles moved at 8.0 μm s^{-1} and V_{pp} was found to be proportional to the numbers of moving SPM particles on the MMA. The optical detector produced a signal of 0.83 mV for a single particle at the frequency of the external magnet field. The background noise was approximately 1.5 mV across the bandwidth of the detector. The MAA detection system allowed us to detect individual SPM beads due to the defined frequency of the signal.

These results allowed us to develop a theoretical framework to describe the sensitivity of this novel magneto-optical detector. The detector signal results from the difference in the intensity of reflected light from the SPM particles positioned over the silicon substrate, P_1, and the micromirrors, P_2 (a list of the reflectivities of aggregates are presented in Table S.3†). The signal from the optical detector, V_{pp}, is linearly related to the effective number of particles, $N(\omega)$, moving in the area of incidence of the laser:

$$V_{pp} = \rho G \Delta P = I_o L S_p \, (R_m - R_s) \, N(\omega), \quad (3)$$

where ρ is the responsivity of the photodetector, G is the transimpedance gain of photodetector, $\Delta P = P_1 - P_2$, I_o is the intensity of the incident light, L is the transmittance of the optical system, S_p is the projected area of an SPM particle on the MMA, and $R_{s,m,b}$ are the reflectivity of the surface, micromirror and particle, respectively. In deriving this equation, we have assumed that R is not a function of particle position and the particles were smaller than the micromirrors and space between the micromirrors. The response of the optical detector is influenced by the motion of the SPM particles on the chip, which we have chosen to express by fitting the measured transport behavior (Fig. S1†) to the function:

$$N = n \, \mathrm{erfc}(\omega \, \omega_c, \sigma), \quad (4)$$

where n is the number of particles in the area of incidence and erfc(ω, ω_c, σ) is the complementary error function centered around the NLM critical frequency, ω_c, as defined by the SPM particle's response to the external magnetic field. At frequencies less than ω_c of the monomers, the value of erfc(ω, ω_c, σ) ≈ 1. Thus, at these low frequencies the optical signal from the MMA was proportional to the intensity of the laser, number of monomers in the area of incidence, size of the beads, and the difference in reflectivity between the mirror and substrate of the MMA. This is consistent with the optical signal measured in Fig. 2c. As the frequency increased the value of erfc(ω, ω_c, σ) decreased until it reached a very small number at a frequency of $\omega_c + \sigma$. This model made it possible to calibrate the optical detection system to determine the number of SPM beads moving across a detection area as a function of the external magnetic field frequency.

Magneto-optical detection of a model protein analyte for the MBA assay

Fig. 3a illustrates the principle of an MBA assay in which a model protein analyte, biotinylated bovine serum albumin

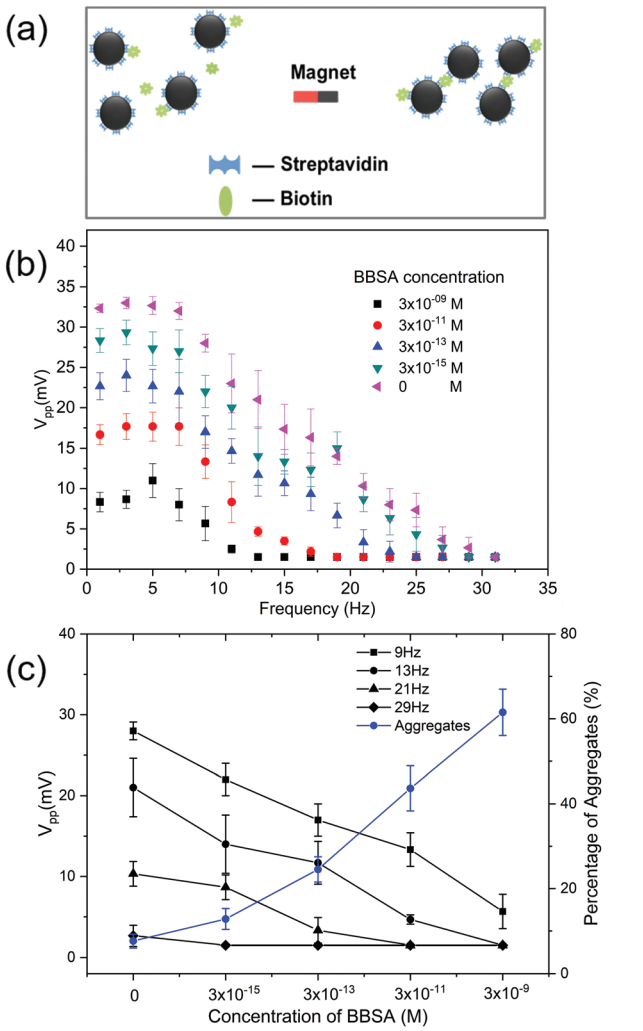

Fig. 3 Demonstration of the micromagnet optical detection scheme based on the model protein biotinylated bovine serum albumin. (a) Schematic of the BBSA magnetic particle assembly assay in which BBSA was detected using streptavidin functionalized SPM particles. The SPM particles were mixed with BBSA for 5 minutes and analyzed after separation from the reaction mixture using a high gradient magnetic field. (b) Micromagnet optical detection of the MBA assay for BBSA concentrations varying between 0 and 3 nM. The V_{pp} signal was observed to decrease as a function of ω for $\omega > \omega_c$ reaching a constant value for $\omega > \omega_i$. The magnitude of V_{pp} was observed to decrease as the concentration of BBSA increased. (c) Analysis of the V_{pp} signal as the concentration of BBSA is increased from 0 to 3 nM. The proportion of particle assembled into aggregates was determined using flow cytometry (detailed description of these results have been presented in the ESI† section). At least 5 measurements are obtained for each data point.

(BBSA), was detected through the formation of biotin–streptavidin SPM particle assemblies. The BBSA MBA assay involved three steps, *i.e.*, BBSA analyte was reacted with the streptavidin SPM particles, a magnetic field was applied to the SPM particles to induce assembly, and the distribution of particles was analyzed using an MMA. We have previously demonstrated that the MBA assay has sub-picomolar sensitivity and can be completed on a flow cytometer in less than 15 minutes.[30] Sensitive detection was achieved on the MMA with optical detection in less than 7 minutes as the reaction takes place in a single step.

Fig. 3b presents the magneto-optical signal, V_{pp}, of the SPM particles for BBSA concentrations varying from 0 to 3×10^{-9} M as ω was increased from 1 to 35 Hz. Three features of the magneto-optical frequency response of the streptavidin-biotin MBA assay are noteworthy. First, the frequency response of the streptavidin particles without BBSA was qualitatively like that of the bare carboxyl beads shown in Fig. 2b, *i.e.*, V_{pp} decreases as a function of ω. The only difference was that the apparent value of ω_c was slightly lower for the streptavidin SPM particles. Second, the V_{pp} signal decreased with the increase in concentration of BBSA, which we attribute to the formation of multimeric bead assemblies. Third, the V_{pp} signal decreased with increasing ω for all the BBSA concentrations tested and reached a steady-state value of approximately 1.5 mV when $\omega > \omega_i$.

Fig. 3c presents the response of the MMA optical detection scheme as a function of BBSA concentration and ω. V_{pp} steadily decreased as the BBSA concentration increased at frequencies less than ω_i. In fact, at frequencies less than 13 Hz the −log(concentration of BBSA) was proportional to ΔV_{pp}, the difference between V_{pp} of the sample with analyte and background. This behavior was closely related to the critical frequency of the SPM beads, *i.e.*, the velocity of the beads decreased at frequencies close to their critical frequency. If we define sensitivity as the concentration at which the absolute value of ΔV_{pp} is greater than three times the standard deviation of the blank, the sensitivity of this MBA assay was 3×10^{-15} M at 5 and 9 Hz. The loss of sensitivity of this detection scheme at higher frequencies was attribute to their lower value of V_{pp} and higher value of the standard deviation of the blanks. Variations in the V_{pp} is associate with to the interaction of the SPM particles with the surface of the MMA and their magnetic properties, *i.e.*, variation in the magnetization of the particles will lead to variation in their transport properties. The aggregation state of the SPM beads was also characterized using flow cytometry to gain an understanding of the mechanism of formation of the magneto-optical signal. The percent of aggregates measured with the flow cytometer is presented as a function of BBSA concentration on the right axis of Fig. 3c. Obviously there was a negative correlation between V_{pp} and the percentage of SPM particle aggregates.

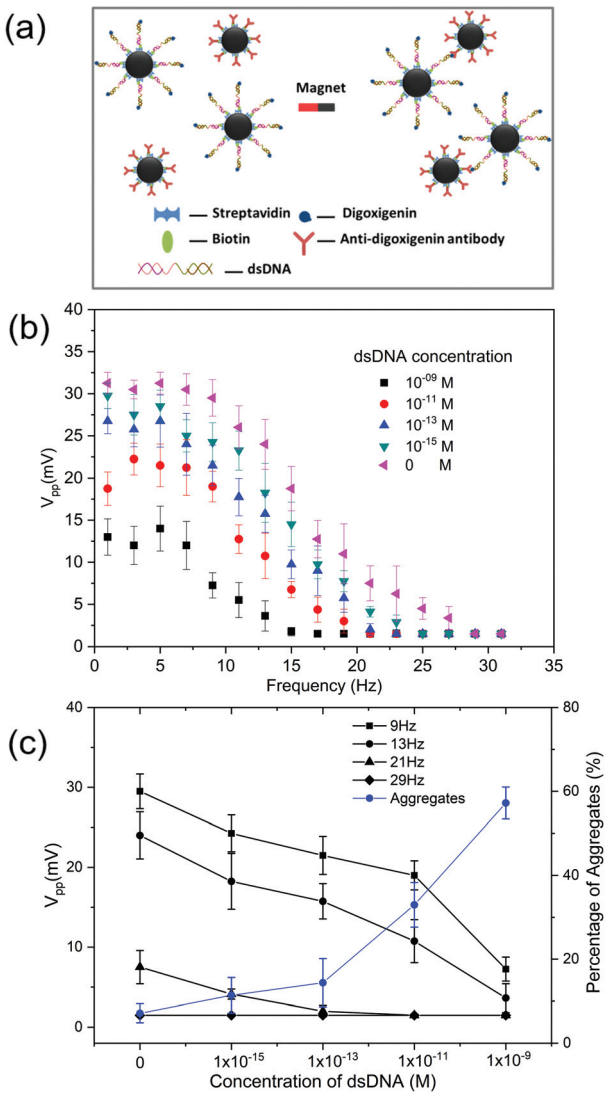

Fig. 4 Detection of the dsDNA *UL27* HSV gene with an MBA assay based on micromagnet optical detection. (a) Schematic of the two-step reaction used to assemble SPM particles. The dsDNA *UL27* gene fragment was first hybridized with oligonucleotide probes labeled with biotin and digoxygenin. The labeled product was separated with streptavidin functionalized SPM particles and then reacted with anti-dig SPM particles to create dimer, trimers, and higher order structures. (b) Micromagnet optical detection of the MBA assay for dsDNA concentrations varying between 0 and 1 nM. The V_{pp} signal was observed to decrease as a function of ω for $\omega > \omega_{c,dimer}$ reaching a constant minimum value for $\omega > \omega_{i,monomer}$. The magnitude of V_{pp} was observed to decrease as the concentration of the *UL27* gene was increased. (c) Analysis of the V_{pp} signal as the concentration of biotin-25mer-dig was increased from 0 to 1 nM. The proportion of particle aggregates was determined using flow cytometry (ESI†). At least 5 measurements are obtained for each data point.

Optical detection of the HSV *UL27* gene based on the MBA assay

Fig. 4a presents a schematic of the principle of detection of the HSV *UL27* dsDNA fragment (75 bp) based on the use of streptavidin and anti-digoxigenin SPM particles for capture and detection. In this detection scheme, the dsDNA target was hybridized with the two complementary oligonucleotides that were functionalized with 5′-digoxigenin and 3′-biotin, respectively. The biotin-labeled reaction product was first extracted with the streptavidin SPM particles and then reacted with the

anti-dig SPM particles. The use of the two affinity labels was found to be essential to achieve a high sensitivity assay, *i.e.*, multimers were not formed when only the biotin label was used. The inhibition of SPM particle reaction appears to result from the immobilization of multiple biotin labels from a single dsDNA fragment with a single streptavidin particle.

The dsDNA MBA assay was characterized as the concentration of dsDNA was varied between 0 and 10^{-8} M using flow cytometry to determine the relative number of monomers and multimers (see ESI† for details of the optimization chemistry). The concentration of aggregates reached at least 20% of the monomers at a dsDNA concentration of 10^{-12} M, as shown in Fig. S2.† The aggregate concentration, however, was dependent on the ratio of streptavidin to anti-dig particles and reaction time. The percentage of aggregates was found to be optimal for a 1 : 1 ratio of streptavidin to anti-dig particles, as shown in Fig. S4.† The percentage of aggregates was optimized for 2 min reaction times, which reflected a rapid rate of reaction achieved for the high particle densities (*i.e.*, 7×10^6 particles per ml). This concentration of particles was selected based on the optimization of the detection of 3′-labled biotin-HSV-1P1 and 5′-labeled dig-HSV-1P1 (presented in the ESI†). This assay was found to be relatively insensitive to high concentrations of background DNA, *i.e.*, the efficiency of the MBA assay decreased by 50% in 10 mg ml^{-1} of nonspecific salmon sperm DNA (Fig. S5†).

Fig. 4b presents the magneto-optical detector response for the reaction of dsDNA concentrations varying from 0 to 1×10^{-7} M as ω was increased from 0 to 35 Hz. The observed change in magneto-optical response was not linked to a change in the number of particles used in the assay, which was held constant at 7×10^6 particles per ml. The results were similar to those observed for the BBSA MBA assay, *i.e.*, the V_{pp} decreased as the concentration of dsDNA added to the particles increased and as the frequency increased. Fig. 4c presents the change of the V_{pp} response as a function of dsDNA concentration at ω ranging from 5 to 29 Hz. The ΔV_{pp} was observed to be proportional to the log of the concentration of dsDNA in the sample. The assay sensitivity was 3×10^{-13} M dsDNA at ω >21 Hz and increased to 3×10^{-15} M dsDNA at 9 Hz. *The* aggregation state of the SPM particles was characterized with flow cytometry (see ESI†) and percent of aggregation is presented on the right axis of Fig. 4c. The ΔV_{pp} response and the percent of SPM particle aggregates were negatively correlated, with the degree of aggregation increasing rapidly at concentrations of dsDNA greater than 10^{-13} M.

NLM transport of SPM particle assemblies

The magneto-optical signal for both the dsDNA and BBSA MBA assays was observed to be sensitive to the frequency of rotation of the external magnetic field, ω. Fig. 5 presents the speed of monomer, dimer and aggregate transport as a function of ω, illustrating a NLM transport response for each of these particle geometries. For the particles prepared from dsDNA, the SPM monomers and dimers had a ω_c of 20 and 15, respectively, and a ω_i of approximately 30 and 21 Hz, respectively. The ω_c and ω_i of particle aggregates were also measured for several particle geometries and were found to be significantly lower than the values measured for dimers. The decrease of ω_c with increasing aggregation number may at first seem counter-intuitive, *i.e.*, eqn (2) indicates that the critical frequency should increase with the radius of the particles. This behavior can be understood in terms of the increase in the size of the aggregates with particle number (sample of aggregate shapes are presented in Table S2†). When the size of the aggregate approached the size of the micromagnet (5 μm) it experienced magnetic fields of varying magnitude and orientation. eqn (2) was derived for a highly simplified model in which the SPM particle moved in the magnetic field potential minimum and it is not valid for large aggregates. This leads us to conclude that the variation in the magnitude and orientation of the magnetic field over an aggregate resulted in a decrease in the net magnetic force and the observed decrease in both the critical and immobilization frequencies.

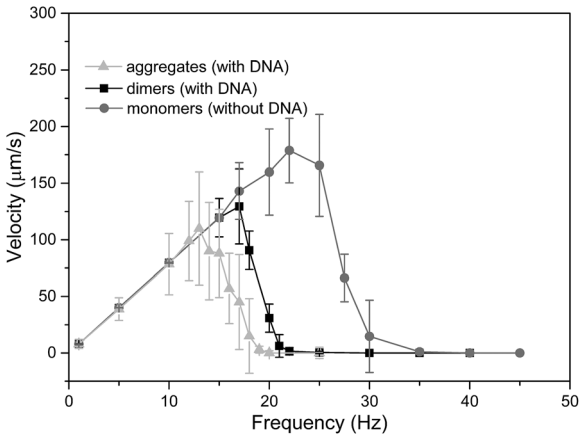

Fig. 5 Average velocity of the monomeric particles, dimers and higher order particle assemblies as a function of the rotation frequency of the external magnetic field. The particles speed was proportional to rotation frequency of the external magnetic field at the frequency below the critical frequency. These measurements were made with at least 15 separated particles using a microscope and high-speed camera.

The response of the MMA magneto-optical detection scheme was observed to vary proportional to −log(analyte concentration) over six orders of concentration of dsDNA and BBSA for ω less than 21 Hz, as shown in Fig. 3c and 4c. This response is useful for *in vitro* diagnostics where a wide dynamic range is highly desirable. The transport of the SPM particles on the MMA was analyzed to identify the mechanism of V_{pp} response (presented in Fig. 3). Optical microscopy confirmed that as the BBSA concentration increased the number of SPM particles decreased and the number of aggregates increased. Most of aggregates formed were dimers with a decreasing fraction of aggregates composed of three, four, and larger numbers of SPM particles. Table S.3† presents an analysis of the reflectivity of the aggregates as a function of geometry and orientation of motion across the MMA. The theoretical analysis of the differential optical reflectivity, ΔP, for the particles positioned between, P_1, and on-top of the micromagnets,

P_2, is based on complete adsorption of light by the SPM particles. Two observations can be made regarding the P values for the different aggregates presented in Table S.3.† First, the ΔP values are highly dependent on the orientation of motion of the aggregates, *i.e.*, dimers have a ΔP of 92.1% or 52.4% for orientations in which their primary axis is normal and parallel to the direction of motion, respectively. This means that ΔP values for a set of particles cannot be determined as the aggregate geometry and orientation of motion were indeterminate. We can, however, see that the aggregates have a lower absolute value of ΔP than monomers and the value decreases as the number of particles in the aggregate increases. These observations are consistent with the decrease in V_{pp} signal as the number monomers decrease and the number of aggregates increased. Thus, the MBA assay and magneto-optical detection scheme used in this study produced a log(concentration) – linear(V_{pp}) that was dominated by the transport of the monomers on the MMA.

Conclusions

Nucleic acid testing (NAT) has become an essential tool for the diagnosis of a range of infectious diseases in healthcare systems, *e.g.*, identification of infectious pathogens, monitoring therapeutic response, and ensuring the safety of blood supplies. NAT combines the advantages of direct and highly sequence-specific detection of the genome of an infectious pathogen with an analytic sensitivity that is several orders of magnitude greater than most antigen detection or virus isolation methods. The use of NAT has significantly reduced the risks of viral transmission during the period between infection and seroconversion of infection with immunovariant viruses,[32] of immunosilent carriage,[33] and of occult carriage.[34] NAT is predominantly performed with PCR amplification in centralized laboratories due to the cost of NAT instruments, their relatively high running costs, and the sophistication of the extraction and amplification procedures required to achieved high specificity and sensitivity. There have been several significant advances in NAT which have allowed POCTs to be performed in multiplex on one or more infectious diseases.[35] First, the development of a number of techniques for isothermal amplification of DNA has significantly simplified sample preparation.[36] Second, detection techniques have been developed around improved amplification techniques that are amenable to POCTs than run in a lateral flow format.[37] Unfortunately, these NAT POC techniques still do not have the sensitivity, specificity or price of operation that can be achieved in centralized laboratories. They also are not amenable to emerging sequencing needs, such as, the detection of 5-methylcytosine modification of DNA for epigenetic profiling.

We have described an integrated MMA-optical detector and used it to detect the HSV *UL27* gene. A MBA assay was used to rapidly separate and detect the *UL27* gene, and this assay was found to work in background DNA and protein concentrations up to 1 mg ml^{-1}. The sensitivity of the magneto-optical detector system was determined by the laser, detector, optical configuration and size and optical properties of the MMA and particles. The detector described was capable if identifying a single 2.8 μm diameter SPM particle and it allowed us to characterize >400 particles per second using a 250-micron diameter laser spot size. Low external magnetic field frequencies (ω) were found to produce high V_{pp}, that was sensitive to the concentration of unreacted monomers, resulting in an assay that operated over six orders of magnitude of dsDNA concentration and had a sensitivity of 3×10^{-15} M dsDNA. This is equivalent to 180 copies of the *UL27* gene in a 0.1 microliter sample volume. In principle, the MMA-optical detector can also be used to detect the products of the MBA assay in several other modes. Direct detection of the aggregates can be performed by implementing NLM separation before detection, *i.e.*, scanning ω between the critical frequencies of the monomers, dimers and higher order aggregates. This technique will have single molecule sensitivity. Multiplexed sensing can also be implemented using multiple color, size or magnetization SPM particles.

The design of an integrated MMA-optical detector instrument will be determined by the analyte, *i.e.*, double or single stranded DNA or RNA, and the application, *i.e.*, POCT *vs. in vitro* diagnostic. We anticipate that four common steps that will be used for these instruments: (1) sample collection, lysis and reaction with oligonucleotide probes; (2) reaction with SPM nanoparticles; (3) magnetic separation of the SPM particles onto the MMA array; and (4) detection of aggregation state of the sample using optical detection. This detection scheme will consume a minimal amount of fluid due to the use of magnetic actuation. The volume of sampling can also be significantly increased by implementing NLM separation before detection, which will allow the number of each type of particle to be determined.[38] The sensitivity of the assay will be determined by the reaction efficiency and the specificity of the analyte-bead reaction. In this article commercial SPM particles was used due to their uniform size, but they are not optimized for high efficiency reactions. Increases in the sensitivity and specificity of the MBA assay can be achieved by using smaller SPM particles, *i.e.*, the rotational diffusion coefficient of a sphere scales as $\propto \frac{1}{r^3}$, and polymer coated SPM particles, which have proven to decrease nonspecific adsorption and decrease background.[39]

In summary, the MMA-optical detector system is a powerful new technology that can be used to collect, separate and detect SPM particles with single particle sensitivity. It appears to be well suited for POCT as it consumes very little fluid and requires relatively low levels of post-acquisition signal processing. We have used this novel system to detect the *UL27* gene from the HSV-1 virus, but it may also be used for rare cell type isolation and the identification of DNA modifications that are not easily detected after amplification.

Conflicts of interest

No conflict of interest to declare.

Acknowledgements

D. Gandhi performed a majority of the MBA experiments; M. Carr and W. Hall designed and optimized the *UL27* nucleic acid probes; M. Mutas and Y. F. Ran developed and optimized the MBA assay; and P. Li, S. Rampini and G. U. Lee microfabricated the MMA, designed the experiments, interpreted the results and prepared the manuscript for publication. We would like to thank the Science Foundation of Ireland (15/IA/3127, 11/TIDA/B2010, 08/IN.1/B2072 TIDA Feasibility 10, and 08/IN1/B2072) for their support. Dr P. Li was supported by the Irish Research Council (IRCSET EMPOWER) and the M. Mutas was supported by the MERC Erasmus Program.

References

1 M. A. M. Gijs, F. Lacharme and U. Lehmann, *Chem. Rev.*, 2010, **110**, 1518–1563.
2 H. Ueda, K. Agatsuma, K. Kajikawa, M. Furuse, S. Fuchino and A. Ishiyama, *IEEE Trans. Appl. Supercond.*, 2009, **19**, 2157–2161.
3 D. R. Baselt, G. U. Lee, M. Natesan, S. W. Metzger, P. E. Sheehan and R. J. Colton, *Biosens. Bioelectron.*, 1998, **13**, 731–739.
4 N. Pamme, *Lab Chip*, 2006, **6**, 24–38.
5 J. Kling, *Nat. Biotechnol.*, 2012, **30**, 578–580.
6 J. Kaiser, *Science*, 2010, **327**, 1072–1074.
7 M. Uhlen, *Nature*, 1989, **340**, 733–734.
8 J. G. Treleaven, J. Ugelstad, T. Philip, F. M. Gibson, A. Rembaum, G. D. Caine and J. T. Kemshead, *Lancet*, 1984, **323**, 70–73.
9 A. van Reenen, A. M. de Jong, J. M. J. den Toonder and M. W. J. Prins, *Lab Chip*, 2014, **14**, 1966–1986.
10 J. R. Lee, D. J. B. Bechstein, C. C. Ooi, A. Patel, R. S. Gaster, E. Ng, L. C. Gonzalez and S. X. Wang, *Nat. Commun.*, 2016, **7**, 12220.
11 S. Kamara, Q. H. Tran, V. Davesne, G. Felix, L. Salmon, K. Kim, C. Kim, A. Bousseksou and F. Terki, *Adv. Mater.*, 2017, **29**, 1703073.
12 J. R. Lee, I. Appelmann, C. Miething, T. O. Shultz, D. Ruderman, D. Kim, P. Mallick, S. W. Lowe and S. X. Wang, *Theranostics*, 2018, **8**, 1389–1398.
13 B. Lim, V. Reddy, X. Hu, K. Kim, M. Jadhav, R. Abedini-Nassab, Y. W. Noh, Y. T. Lim, B. B. Yellen and C. Kim, *Nat. Commun.*, 2014, **5**, 3846.
14 D. J. B. Bechstein, E. Ng, J. R. Lee, S. G. Cone, R. S. Gaster, S. J. Osterfeld, D. A. Hall, J. A. Weaver, R. J. Wilson and S. X. Wang, *Lab Chip*, 2015, **15**, 4273–4276.
15 B. Lim, S. R. Torati, K. W. Kim, X. Hu, V. Reddy and C. Kim, *NPG Asia Mater.*, 2017, **9**, e369.
16 S. Rampini, P. Li and G. U. Lee, *Lab Chip*, 2016, **16**, 3645–3663.
17 G. Vieira, T. Henighan, A. Chen, A. J. Hauser, F. Y. Yang, J. J. Chalmers and R. Sooryakumar, *Phys. Rev. Lett.*, 2009, **103**, 128101.
18 M. Donolato, P. Vavassori, M. Gobbi, M. Deryabina, M. F. Hansen, V. Metlushko, B. Ilic, M. Cantoni, D. Petti, S. Brivio and R. Bertacco, *Adv. Mater.*, 2010, **22**, 2706–2710.
19 B. B. Yellen, R. M. Erb, H. S. Son, R. Hewlin, H. Shang and G. U. Lee, *Lab Chip*, 2007, **7**, 1681–1688.
20 P. Li, D. Kilinc, Y.-F. Ran and G. U. Lee, *Lab Chip*, 2013, **13**, 4400–4408.
21 S. Rampini, D. Kilinc, P. Li, C. Monteil, D. Gandhi and G. U. Lee, *Lab Chip*, 2015, **15**, 3370–3379.
22 P. Chayavichitsilp, J. V. Buckwalter, A. C. Krakowski and S. F. Friedlander, *Pediatr. Rev.*, 2009, **30**, 119–130.
23 K. L. Tyler, *Herpes*, 2004, **11**(Suppl. 2), 57A–64A.
24 R. F. Itzhaki, *FASEB J.*, 2017, **31**, 3216–3226.
25 J. W. Tang, M. Lin, L. Chiu and E. S. Koay, *J. Med. Virol.*, 2010, **82**, 1911–1916.
26 M. Koenig, K. S. Reynolds, W. Aldous and M. Hickman, *Diagn. Microbiol. Infect. Dis.*, 2001, **40**, 107–110.
27 C. Gardella, M.-L. Huang, A. Wald, A. Magaret, S. Selke, R. Morrow and L. Corey, *Obstet. Gynecol.*, 2010, **115**, 1209–1216.
28 M. J. Slomka, L. Emery, P. E. Munday, M. Moulsdale and D. W. G. Brown, *J. Med. Virol.*, 1998, **55**, 177–183.
29 L. Verano and F. J. Michalski, *J. Clin. Microbiol.*, 1995, **33**, 1378–1379.
30 Y.-F. Ran, C. Fields, J. Muzard, V. Liauchuk, M. Carr, W. Hall and G. U. Lee, *Analyst*, 2014, **139**, 6126–6134.
31 T. Ukai, H. Morimoto and T. Maekawa, *Phys. Rev. E: Stat., Nonlinear, Soft Matter Phys.*, 2011, **83**, 061406.
32 S. M. Zou, S. L. Stramer and R. Y. Dodd, *Transfus. Med. Rev.*, 2012, **26**, 119–128.
33 I. Loussertajaka, F. Brunvezinet, F. Simon, T. D. Ly, M. L. Chaix, S. Saragosti, A. M. Courouce and D. Ingrand, *Lancet*, 1994, **343**, 1393–1394.
34 D. Candotti, Y. Adu-Sarkodie, F. Davies, E. Baldrich-Rubio, K. Stirrups, H. Lee and J. P. Allain, *J. Med. Virol.*, 2000, **62**, 1–8.
35 A. V. Ritchie, I. Ushiro-Lumb, D. Edemaga, H. A. Joshi, A. De Ruiter, E. Szumilin, I. Jendrulek, M. McGuire, N. Goel, P. I. Sharma, J. P. Allain and H. H. Lee, *J. Clin. Microbiol.*, 2014, **52**, 3377–3383.
36 A. Niemz, T. M. Ferguson and D. S. Boyle, *Trends Biotechnol.*, 2011, **29**, 240–250.
37 M. A. Dineva, D. Candotti, F. Fletcher-Brown, J. P. Allain and H. Lee, *J. Clin. Microbiol.*, 2005, **43**, 4015–4021.
38 P. Li, D. Kilinc, Y. F. Ran and G. U. Lee, *Lab Chip*, 2013, **13**, 4400–4408.
39 G. U. Lee, S. Metzger, M. Natesan, C. Yanavich and Y. F. Dufrene, *Anal. Biochem.*, 2000, **287**, 261–271.

